How colloid nature drives the interactions between actinide and carboxylic surfactant in sol: Towards a mesostructured nanoporous actinide oxide material

Zijie Lu, Thomas Zemb, X. F Le Goff, Joseph Lautru, Hassan Khoder, Diane Rébiscoul

Version of Record: https://www.sciencedirect.com/science/article/pii/S0021979723000991
Manuscript_12f0feddddfc6d1764a4f8236d43e965

How colloid nature drives the interactions between actinide and carboxylic surfactant in sol: towards a mesostructured nanoporous actinide oxide material

Zijie Lu[1], Thomas Zemb[1], Xavier Le Goff[1], Joseph Lautru[1], Hassan Khoder[1], Diane Rébiscoul[1*]*

[1] Institut de Chimie Séparative de Marcoule, CEA, UMR 5257 CEA-CNRS-UM-ENSCM, 30207 Bagnols-sur-Cèze, France.

Corresponding authors: zijie.lu@cea.fr ; tel: 0033 4 38 78 45 50; diane.rebiscoul@cea.fr; tel: 0033 4 66 33 93 30

ABSTRACT

Hypothesis

The key to prepare a mesostructured porous material by a soft-template route coupled to a colloidal sol-gel process is to control the surfactant-colloid interface. In the case of tetravalent actinide ions, their high reactivity in aqueous media always leads to uncontrolled and irreversible condensation. The addition of a complexing agent to the sol may moderate these reactions and enhances the interaction between the colloids and the surfactant to *in fine* prepare a mesostructured nanoporous actinide oxide material.

Experiments

Several colloidal sols were prepared without and with formic acid as complexing agent by varying the molar ratios between thorium, carboxylic surfactant and pH. Small and Wide Angle X-ray Scattering were used to characterize the nature of the colloids, their interaction with the surfactant and the final ThO_2 materials.

Findings

Depending on the colloid nature, hexagonal or worm-like hybrid mesophase is formed. The thermal treatment of the worm-like mesophase with a sufficient amount of Th-formic acid hexameric species coated at the surface of surfactant micelles generates micrometric ThO_2 nanofibers. This material having an accessible porosity opens new perspectives to be impregnated with minor actinide solutions offering a promising safety method for the fabrication of mixed oxide nuclear fuel and the minor actinide transmutation.

KEYWORDS: colloidal sol-gel, actinide colloid, carboxylic surfactant, Small Angle X-ray Scattering

INTRODUCTION

Even if a wide variety of mesostructured porous oxide materials prepared with f-block elements are available in the literature [1-7], their colloidal sol-gel chemistry coupled to soft-templating approach in aqueous solution is still poorly investigated. More particularly, the interaction between surfactant molecules and primary colloidal precursors formed with high density elements remains unknown. Indeed, the key to prepare a mesostructured porous material

by a soft-template route coupled to a colloidal sol-gel process is to control the surfactant-colloid interface[8].

The use of such route is of interest for mixed oxide nuclear fuel preparation currently used and for the transmutation of minor actinides in Generation IV reactors. Indeed, mesostructured porous actinide oxides such as ThO_2 or UO_2, having accessible and connected pores can be easily impregnated by various concentrated actinide solutions. This simple process leads to the formation of nuclear fuels having a homogeneous distribution of actinides at a nanometric scale avoiding "hot spot" formation due to local accumulation of more fissile elements. More particularly, the combination of aqueous colloidal sol-gel process and surfactant-based soft-templating method for the preparation of mesostructured and porous actinide oxides is a promise way. This liquid route reduces the manipulations of radioactive powders comparing with the traditional metallurgical route leading to a safer fabrication. However, this type of synthesis route is still a big challenge due to the complex behavior of tetravalent actinides An(IV) in aqueous solution. Indeed, due to their high electron density and high valence, the tetravalent actinide ions An^{4+} have a high reactivity in aqueous media, which always leads to uncontrolled and irreversible condensation[9, 10]. To form a well-defined precursor-surfactant hybrid interface and furthermore an ordered mesophase, the hydrolysis-condensation of actinide precursors has to be controlled and the interaction between An(IV) and the surfactants has to be enhanced[8, 11].

Herein, we study the interaction between carboxylic surfactant with various thorium colloids for the synthesis of mesostructured nanoporous ThO_2 materials by a colloidal sol-gel route coupled with soft-templating method. To reach this goal, we have used two colloidal strategies: one without controlling the Th colloidal species and another reducing the activity of Th species using Formic Acid (FA) as complexing agent as in our previous work[12]. To control the

mesostructure, a carboxylic surfactant belonging to the so-called AKYPO surfactant family was chosen for the high reactivity of the carboxylic acid termination enabling a strong interaction with inorganic precursors[13] and its remarkable stability in hard water and high salinity conditions[14, 15]. In a preliminary study devoted to uranium oxide, it has been demonstrated that the strong complexation between AKYPO and tetravalent uranium U(IV) leads to the formation of a stable organized mesophase with well-defined precursor-surfactant interface[16, 17], without producing any final material. In addition, the roles of the key synthesis parameters such as the molar ratios between each component (Th, AKYPO and FA), pH and the post-synthesis thermal treatment have been investigated to find out the optimal conditions for the consolidation of a robust ordered mesophase. Using Small and Wide Angle X-ray Scattering (SAXS/WAXS) and Scanning and Transmission Electron Microscopies (SEM and TEM), we evidenced the effect of the nature and of the size distributions of the colloids on their interaction with AKYPO and thus, on the final structure of the mesostructured nanoporous ThO_2 materials.

MATERIALS AND METHODS

Materials

AKYPO RO 90 VG (Polyoxyethylene(9) oleyl ether carboxylic acid, $C_{16/18:1}E_9COOH$, Mw = 722 g/mol) labeled as AKYPO from Kao Chemicals was used as received. Thorium nitrate pentahydrate ($Th(NO_3)_4.5H_2O$), formic acid (HCOOH) from Sigma Aldrich were used as received.

Methods

Thorium chloride solution (Th solution) was prepared by the dissolution of $Th(NO_3)_4.5H_2O$ in 4 M HCl solution. The prepared solution was heated at 60 °C until the complete removal of water and the obtaining of a dry residue. Afterwards, this dry residue was dissolved in 4 M HCl solution

and this operation was repeated at least three times in order to completely remove nitrate from the solution. Then, the final dry residue was dissolved again in 4 M HCl solution. The concentration of the final solution was analyzed by ICP-AES and a concentration of [Th] = 0.37±0.01 M was obtained.

Th-FA colloidal sols were prepared by indirect precipitation. For this, 2.5 mL of Th solution ([Th] = 0.37 M) was added dropwise into 2 mL of FA (formic acid) solution at various concentrations corresponding to the following ratio Th/FA: 0.05, 0.25 and 0.5. After each drop addition, the pH value of the colloidal dispersions was corrected by adding a solution of 10 M NH_4OH to maintain the solutions at four fix pH values: 2.5, 3.5, 4.5 and 5.5. Th solutions with a concentration of 0.1 M were prepared at the same pH values as references.

Th-AKYPO and Th-FA-AKYPO sols were prepared by indirect precipitation[18]: Th solution was added dropwise into 5 mL of solutions with different concentrations of AKYPO and FA to obtain varied molar ratios of Th/AKYPO and Th/FA. After each drop, the pH value of the solution was maintained around pH = 3.5 by addition of 10 M NH_4OH. Flocculation was observed upon the addition of Th solution. The obtained flocs were filtered, preheated at 80 °C and thermally treated at 450 °C for 5 h to remove organic components and obtain the final material.

Characterizations

Small-angle and Wide-angle X-ray Scattering (SAXS/WAXS) analysis were carried out in transmission geometry with a Xenocs setup equipped with a Mo anode (λ = 0.71 Å) using a MAR345 2D imaging plate detector. Such short wavelength allows the probing of a scattering range from few angstroms to 30 nm and at the same time. The collimation was ensured by a Fox2D multilayer mirror and by a set of scatterless slits that delimitated the beam to a square section (0.8

mm side length at the sample position). The distance from the sample to the detector was about 750 mm and was calibrated using silver behenate powder. Sols were analyzed in glass capillaries of 2 mm of diameter. X-ray absorbing actinides powders were analyzed in glass capillaries of 1mm of diameter. Gel-like samples were analyzed between two foils of Kapton. Azimuthal averaging of 2D-data recorded by a MAR345 imaging plate detector was performed using the FIT2D software taking into account the electronic background of the detector, the empty cell subtraction and an intensity calibration. The scattered intensity in absolute scale (in cm^{-1}) was expressed versus the magnitude of the scattering vector $q = \frac{4\pi\sin\frac{\theta}{2}}{\lambda}$, where θ was the scattering angle. Experimental resolution was $\Delta q/q = 0.02$. Scanning electron microscopy (SEM) and Transmission electron microscopy (TEM) were carried out for the analyses of final materials. SEM analyses were performed on a FEI QUANTA 200 ESEM FEG operating at 15 kV equipped with an Everhart-Thornley detector. TEM analyses were performed at 200 kV on a Jeol200CX TEM equipped with a Photonic-Science camera.

RESULTS AND DISCUSSION

Determination of Th species

To determine how the presence of formic acid (FA) controls the speciation of Th, colloidal sols have been prepared and analyzed at different pH and Th/FA ratios. All the sols obtained were transparent except the sol with a molar ratio Th/FA = 0.5 at pH = 5.5 and the solutions without FA (Th solutions) from pH $\geq$ 3.5 which were translucent. The Th solutions became turbid from pH > 3.5. The sols and Th solutions were analyzed by SAXS/WAXS and the results are presented in **Figure *1***.

For the Th solutions, the scattering intensity increases with pH (**Figure *1*** (a)). At pH = 2.5, the low scattering intensity in all q range (~ 0.2 cm^{-1}) indicates that Th species at this pH are all soluble and undetectable by SAXS. These soluble species can correspond to Th^{4+} or $ThCl_3^+$ as depicted by the speciation diagram of Th in chloride media presented in **Figure S1 (a) and (b)**. When pH = 3.5, the SAXS pattern presents a Guinier-type regime around q = 0.4 nm^{-1} characteristic of colloids in solution. These Th hydroxyl colloids $Th_x(OH)_y^{(4x-y)+}$ may correspond to a mixture of Th^{4+}, $Th_2(OH)_3^{5+}$, $Th_2(OH)_2^{6+}$, $Th_4(OH)_8^{8+}$, $Th_6(OH)_{15}^{8+}$ and $Th_6(OH)_{14}^{10+}$ according to the speciation diagrams (**Figure S1 (a) and (b)**).

When pH ≥ 4.5, the scattering intensity follows a power-law form varying from $q^{-1.77}$ to q^{-2} indicating the formation of Diffusion-limited Aggregation (DLA) typed fractal aggregates[19]. Indeed, at this pH the condensation of $Th_x(OH)_y^{(4x-y)+}$ and the aggregation of ThO_2 nanoparticles ($Th_xO_y(OH)_z(am)$) are favored[20-22] forming a gel.

The SAXS patterns of the sols presented on **Figure *1*** (b) to (d) present a plateau from q = 4 nm^{-1} except for the samples with Th/FA = 0.5 at pH = 4.5 and 5.5. For these two samples, the intensity reaches a plateau for lower q value (~ 0.2 nm^{-1}). When pH = 2.5, whatever the Th/FA ratio, the SAXS patterns have a scattering intensity lower than 0.1 cm^{-1}, indicating the low condensation degree of the system. Analogous to the Th solution, at this pH value, Th species may be in form of Th^{4+} and $ThCl_x(HCO_2)_y^{(4-x-y)+}$ (with $x+y \leq 3$), that are not detectable by X-ray scattering. When pH > 2.5, the scattering intensity of the plateau increases with the pH but the magnitude of this increase is more and more moderate with the increase of FA concentration (**Figure *1*** (b) to (d)). Indeed, at the same pH, the scattering intensity decreases with Th/FA ratio. This underlines that the addition of FA inhibits the formation of $Th_x(OH)_y^{(4x-y)+}$ and prevents from

their aggregation as observed in Th solutions. This is mainly due to the formation of Th-FA complexes with a hexameric Th core and a shell of $HCOOH/HCOO^-$ [23-25] (**Figure *1*** (e)).

To determine the distribution of these species, SAXS patterns have been simulated (**Figure *1*** (e)) taking into account two types of objects: (i) Th-FA hexameric complexes simulated as a core-shell object and (ii) $Th_xO_y(OH)_z(am)$ colloids simulated as an ellipsoid having ThO_2 scattering length density. Since the size and the scattering length density (SLD) of FA are negligible compared with those of ThO_2, it was not necessary to take into account FA as a shell for ThO_2 object. The form factors of the Th species, their scattering length density differences (ΔSLD) and their sizes for the simulation are presented in **Table S1** to **Table S3**. These simulation results supplying the distribution of species in the solutions and the sols as a function of the pH and Th/FA are illustrated on the **Figure *1*** (e).

Without FA and pH = 3.5, almost 70% of Th formed polydisperse ThO_2 nanoparticles ($Th_xO_y(OH)_z(am)$) with a size varying from 1.2 to 5.2 nm. When pH $\geq$ 4.5, the system formed fractal aggregates. The fractal dimensions increased from 1.75 to 1.95 as pH increased from 4.5 to 5.5, corresponding to the Diffusion-limited Aggregation (DLA)[19]. Moreover, the gyration radius of the primary particles increases from 9.5 nm to 12 nm. This indicates that the increase of pH promotes the growth of ThO_2 nanoparticles and leads to the formation of denser aggregates. When FA is added, a moderate condensation level is required for the formation of Th hexamer[26], here it occurs when Th/FA $\geq$ 0.25 or pH $\geq$ 3.5. The fraction of Th-FA hexameric complexes increases with the increase of pH and/or the increase of Th/FA ratio. When the system is at a high pH (pH = 5.5) or high Th/FA ratio (Th/FA = 0.5), the condensation of Th species are largely promoted leading to the formation of colloidal ThO_2 nanoparticles. The size and polydispersity of these nanoparticles increase with pH.

Interaction between Th species and AKYPO

Th-AKYPO systems: from colloidal micelles to hexagonal mesophase

Before the addition of Th solution, the SAXS pattern of 0.1 M AKYPO solution (**Figure *2*** (a)) corresponds to the scattering signal of core-shell objects as already observed in our previous work[17]. When Th is added to the sol, *i.e*. from Th/AKYPO = 0.14 (pH = 3), two changes can be noticed. First, the scattering peak shifts to higher q region indicating the shrinkage of core-shell micelles due to the dehydration of their head groups. Second, the scattering intensity increases between q = 2 nm^{-1} to q = 8 nm^{-1} due to the presence of $Th_x(OH)_y^{(4x-y)+}$ and ThO_2 nanoparticles ($Th_xO_y(OH)_z(am)$). According to the speciation diagram of Th in water at a concentration of [Th] = 0.03 M (**Figure S1 (a)),** $Th_x(OH)_y^{(4x-y)+}$ species at pH = 3 may correspond to Th^{4+}, $Th_2(OH)_2^{6+}$ and $Th_2(OH)_3^{5+}$.

The sol becomes more viscous when the Th/AKYPO ratio increases. This is associated to an increase of the concentration of polynuclear species complexed by the acidic function of AKYPO locating on the shell of micelles. This leads to the structural transition from core-shell to cylindrical micelles[27] by a decrease of the equilibrium area per head a_0 and leading to the decrease of the packing parameter P_0 (**Figure *2*** (b)). This is highlighted by the refinement of the shoulder at q = 1.5 nm^{-1} for the sol at Th/AKYPO = 0.2.

From Th/AKYPO ≥ 1.25, a white floc is obtained at the bottom of the vial having similar SAXS patterns (**Figure *2*** (a) and **Figure *3*** (c)) presenting two scattering orders with $q_1:q_2 = 1:\sqrt{3}$ that indicate the formation of a hexagonal structure. In water-AKYPO binary, the hexagonal phase is formed from 40 to 60 wt% with a characteristic distance of the first scattering order d_{10} comprised between 7.3 and 6.5 nm. In this Th-AKYPO system, the hexagonal phase is formed at much lower AKYPO concentration (< 8 wt%) with a smaller d_{10} of 6.3 nm. These demonstrate

that the presence of $Th_x(OH)_y^{(4x-y)+}$/$Th_xO_y(OH)_z$(am) dispersed between cylinders act as a "glue" to bridge partially adjacent cylinders as illustrated on **Figure *2*** (b). In addition, two sharp diffraction peaks corresponding to NH_4Cl are observable at high q when Th/AKYPO = 0.2. They disappear when Th/AKYPO = 1.25 *i.e* when a phase separation occurs. This may be due to the solubilization of NH_4Cl in the aqueous phase of the supernatant.

Role of FA in the AKYPO mesophase formation

To investigate the effect of the complexing agent and thus the effect of Th-FA hexameric complexes ($Th_6(OH)_4O_4(HCOO)_{12}$) on the structuration of Th-AKYPO mesophase, SAXS analyses have been performed on two systems Th-AKYPO and Th-FA-AKYPO with Th/AKYPO at pH = 3. To ensure of the formation of Th-FA hexameric complexes in Th-FA-AKYPO system, Th/FA = 0.1 (**Figure *1*** (e)). The SAXS patterns of the flocs and the supernatants of these two systems with Th/AKYPO = 1.25 are shown in **Figure *3*** (a) and (b).

The SAXS patterns of two flocs both present a hexagonal phase with sharp first scattering orders. The second scattering order of Th-FA-AKYPO system is sharper than the one of Th-AKYPO, which is partially covered by the scattering shoulder of $Th_x(OH)_y^{(4x-y)+}$/ $Th_xO_y(OH)_z$(am) around q = 2 nm^{-1}. Furthermore, the SAXS pattern of the supernatant of Th-AKYPO system (**Figure *3*** (a)) presents a scattering oscillation around q = 1 nm^{-1} and a shoulder from q = 2 to 8 nm^{-1}. These two signals can be respectively assigned to the residual AKYPO micelles and $Th_x(OH)_y^{(4x-y)+}$ generated by the uncontrolled hydrolysis of Th. In the SAXS pattern of the supernatant of Th-FA-AKYPO system (**Figure *3*** (b)), only a signal of $Th_x(OH)_y^{(4x-y)+}$ species is observable. Considering the experimental conditions, this indicates that all AKYPO micelles interact with Th-FA hexameric species to form the hexagonal structure. The comparison of these

two systems reveals that the addition of FA promotes the interaction between Th species and AKYPO micelles.

To further confirm the promoting role of FA in the interaction of Th and AKYPO, SAXS analyses have been carried out on the flocs obtained from these two systems varying Th/AKYPO ratio from 1.25 to 5 at pH = 3. The SAXS patterns of the flocs are shown in **Figure *3*** (c) and (d).

For Th-AKYPO system (**Figure *3*** (c)), the increase of Th/AKYPO from 1.25 to 5 had no significant effect on the structuration of the mesophase. The flocs present a hexagonal phase with a characteristic distance of (10) plane d_{10} = 6.3 nm. In fact, in this system without FA, the interaction of Th and AKYPO micelles are always in competition with the hydrolysis-condensation of Th species. The increase of Th/AKYPO cannot promote the interaction between Th precursors and AKYPO micelles. In this case, the structuration of hybrid mesophase does not depend on Th/AKYPO ratio but the charge matching[28] between the $Th_x(OH)_y^{(4x-y)+}$ species and AKYPO micelles.

For Th-FA-AKYPO system (**Figure *3*** (d)), when Th/AKYPO $\leq$ 2.5, the flocs present a hexagonal phase with d_{10} = 7 nm. When this ratio increases to 5, this distance d_{10} reaches 4.7 nm with the disappearance of the second scattering order indicating a phase transition from hexagonal structure to entangled worm-like structure. Moreover, the increase of scattering intensity at low q following a power-law form of $q^{-2.8}$ is characteristic of fractal surface[19] generated by Th-FA hexameric complexes accumulated at the surface of AKYPO micelles. The sharp diffraction peaks in high q range are assigned to the crystallization of $ThCl_x(OH)_y(HCO_2)_z$. In this system, the addition of FA controls the Th speciation and benefits the formation of Th hexameric species. These polynuclear species have a better interaction with AKYPO than $Th_x(OH)_y^{(4x-y)+}$ favoring the

formation of a denser inorganic skeleton in the hybrid network when Th concentration increases. This is essential to form a rigid and consolidated structure. The rigidity of hexagonal phase (Th/AKYPO = 1.25) and entangled worm-like structure (Th/AKYPO = 5) has been studied and will be discussed in the following section.

Consolidation of the mesophase

To synthesize mesostructured materials, the consolidation of the mesophase is always a crucial before the removal of surfactant[8]. To our best knowledge, no consolidation method has been proposed for any actinide oxide. Depending on the system (Th-AKYPO or Th-FA-AKYPO) and thus the Th species, different strategies have been used and the structures of final material obtained based on these strategies will be compared and discussed in the following section.

For Th-AKYPO system, the condensation of Th species ($Th_x(OH)_y^{(4x-y)+}$/ $Th_xO_y(OH)_z$(am)) between the cylindrical micelles was promoted by increasing the pH of the sols from 2.3 to 8 (see **Figure *4*** (a) and (b)).

As highlighted by the **Figure *4*** (a), the scattering patterns are strongly influenced by the pH. The origin of the phenomenon comes from the interactions between AKYPO and the various Th species existing in solution. Indeed, as presented in the speciation diagram of Th in **Figure S1** and **Figure *1*** (e), the predominant species in solution varied as a function of pH due to the modification of the hydrolysis-condensation reaction. When pH is between 2.3 and 3, the predominant specie is $Th_2(OH)_2^{6+}$. When pH > 4, the saturation index of amorphous thorium oxide becomes positive[29, 30], therefore the predominant species at pH = 8 are $Th_xO_y(OH)_z$(am) having various size. When the pH increases from 3 to 8, the first scattering order shifts to high q region with the disappearance of the second scattering order. Furthermore, the increasing scattering in

low q region follows a power-law of $q^{-1.95}$, indicating the formation of fractal aggregates of $Th_xO_y(OH)_z$(am). The sharp peaks in wide angle region are due to the crystallization of NH_4Cl during the adjustment of pH. These results highlight that the increase of pH promotes the condensation of Th species that modifies the mesophase. Indeed, the increase of pH favors the growth of $Th_xO_y(OH)_z$(am) wrapping around AKYPO micelles. Therefore, the configuration of hybrid Th-AKYPO interface needs to modify due to the charge matching principle[28]. This leads to a phase transition from hexagonal phase to entangled worm-like structure. For hexagonal arrays, the distance between two adjacent cylinders h is a characteristic parameter to have an insight to their rigidity (see **Figure *2*** (b)). For the AKYPO-water binary system, h decreases from 2.4 nm to 1.2 nm when the mass fraction of AKYPO increases from 40% to 70% (**Figure S2** (b)). In Th-AKYPO system, h decreased from 1.2 nm to 0.5 nm when pH increased from 3 to 8 proving the consolidation of the hybrid mesophase.

For Th-FA-AKYPO system with Th/FA = 0.1, the consolidation of the mesophases can be done by the increase of Th/AKYPO from 1.25 to 5. This is confirmed by studying the thermal stability of two samples, Th/AKYPO = 1.25 and 5, after a preheating of 80 °C for 2 h (**Figure *4*** (c)). After the preheating of the sample prepared at Th/AKYPO = 1.25, the first scattering order shifted from q = 0.9 nm^{-1} to 1.2 nm^{-1}, indicating the shrinkage of the structure due to a dehydration of the head groups of AKYPO. This shrinkage goes with the loss of the second scattering order and the appearance of three sharp peaks from q = 4 nm^{-1} to q = 7 nm^{-1} probably characteristic of the crystallization of Th-FA hexameric complexes. The equilibrium distance between two adjacent cylinders h decreases sharply from 2.1 nm to 0.2 nm. These modifications deformed the cylindrical micelles, converting the hexagonal mesophase to a bicontinuous phase with entangled worm-like micelles. Unlike the sample with Th/AKYPO = 1.25, the SAXS pattern of the sample prepared at

Th/AKYPO = 5 only had a slight shift of the scattering peak from q = 1.3 nm^{-1} to q = 1.4 nm^{-1} after the preheating. The distance related to the first scattering peak had a slight decrease of 0.2 nm. Indeed, the mesophase synthesized at Th/AKYPO = 5 was embedded by more Th-FA hexameric species and contained less water compared to the one prepared at Th/AKYPO = 1.25. This leads to a more rigid inorganic network remaining stable during its preheating. These results confirm that for Th-FA-AKYPO system, the entangled worm-like structure formed at Th/AKYPO = 5 is more rigid than the hexagonal mesophase prepared at Th/AKYPO $\leq$ 2.5.

Final materials

Morphology and structure

To remove organic components, all flocs were thermally treated at 450 °C for 5 h under air with a ramp of 5 °C/min based on our previous work[16]. The powder obtained have been analyzed by SAXS, SEM and TEM. The results are presented on **Figure 5**.

The SAXS patterns of the final materials from all systems present a broad scattering peak from q = 0.3 nm^{-1} to q = 3 nm^{-1}. These broad scattering peaks are characteristic of a loose packing of ThO_2 nanoparticles with a bicontinuous interparticular porosity. Such broad scattering peaks have been already shown in the SAXS analyses of other mesoporous materials such as biomass derived absorbent[30], biochar[30] and mesoporous oxides[31, 32]. The presence of these nanoparticles is also attested by the two diffraction peaks at q = 19.6 nm^{-1} and q = 22.5 nm^{-1} present on the SAXS patterns associated with the crystalline planes (111) and (200) of the fluorite-type structure of ThO_2[33]. The average sizes of the crystallites deduced from the Scherrer equation are comprised between 2.5 and 6 nm (**Table S4**). In addition, the SAXS patterns of Th-A-1.25-8 and Th-F-A-5 follow a power-law around q^{-2} in low q region (q = 0.2 to 0.4 nm^{-1}) indicating the

presence of aggregates with fractal surface corresponding to characteristic distances between 6 and 30 nm.

All of these results are consistent with the TEM images shown on **Figure 5** presenting two different morphologies: (i) a bicontinuous nanoporous assembly of ThO_2 nanoparticles (**Figure 5** (b), (c) (d), (e) and (g)) and (ii) rod-like assemblies of ThO_2 nanoparticles (**Figure 5** (e) and (i)). This last morphology is also observable at a microscale as attested by the SEM image of the material Th-F-A-5 (**Figure 5** (j)) showing a set of micrometric fibers. These fibers present a porous volume of 0.22 $cm^3.g^{-1}$ and two types of pores, micropores and mesopores as attested by water adsorption-desorption isotherms using dynamic water vapor sorption (DVS) (see **Figure SI3**). The micropores may correspond to interparticular voids between ThO_2 nanoparticles forming the cylindrical wall and the mesopores can be assigned to the porosity generated by the AKYPO templating. The presence of these mesopores makes easy the microporosity accessibility to water. Such experiment highlights the accessibility of the porosity to an aqueous phase and suggests the possible impregnation of ThO2 with actinide solutions.

How the interactions between colloids and AKYPO drives the mesostructuration in the final materials

The formation of these two morphologies are related to the rigidity of the mesophases before the thermal treatment. Indeed, the first morphology is obtained when the amount of Th species in the mesophase is insufficient and/or their sizes are not homogenous. This is the case when pH $<$ 8 for the system without or Th/AKYPO $\leq$ 2.5 when FA is present. The second morphology is obtained when the Th species amount is sufficient and their size homogeneous (Th-F-A-5). Without FA, even if the condensation of Th species is promoted as at pH=8 forming

nanoparticles of $Th_xO_y(OH)_z(am)$ in the hybrid network, the interaction between AKYPO molecules and Th species with various size and condensation degree are still not sufficiently enhanced to provide a robust inorganic network for the complete conservation of the cylindrical arrays during the thermal treatment. This leads to a mixed morphology of (i) and (ii) (see **Figure 5** (e)). In presence of FA, Th-FA hexameric complexes with homogenous size and condensation degree are formed and the interaction between these colloidal precursors and AKYPO molecules are optimized. Therefore, if their amount are sufficient to align along the worm-like micelles (Th/AKYPO = 5), they maintain the cylindrical mesostructure during the thermal treatment. In that case, only rod-like assemblies of ThO_2 nanoparticles presenting micropores and mesopores are obtained.

CONCLUSION

For the first time, we have shown how the nature of the actinide colloid influences the surfactant-colloid interaction and ultimately, how this behavior impacts the mesostructure of final actinide oxide material.

We have evidenced that the addition of a complexing agent plays an important role on the structuration of Th-based mesophases. This results are consistent with the findings cited in the review of Sanchez *et al.* for transition metals and other high valence elements[8, 34]. We have shown that Th-FA complexes having uniform size and condensation degree have strong interaction with soft-template molecules. This leads to the formation and the conservation of sufficiently rigid mesophase after the thermal treatment. The findings provide an useful preliminary guidance for synthesis of mesoporous materials from transition metal[34-36] to lanthanides[2-6] and actinides with higher density. However, one property still need to be measured: the charge of the colloidal precursors, *i.e.* the zeta potential. Indeed, it has been demonstrated that the matching of charge

density at the precursor/surfactant interfaces pilots the self-assembly process [37, 38]. This can be controlled by adjusting the pH of the solution to influence the charge of the precursors.

In addition, the final material prepared in this work presents a sufficient accessible porosity. The impregnation of these pores with minor actinide solutions is a promising safety method for the fabrication of mixed oxide nuclear fuel. Comparing with the conventional metallurgical route[39-41], this liquid route reduces the manipulations of radioactive powders leading to a safer fabrication. Furthermore, the high homogeneity of actinides distribution avoids "hot spot" formation within the nuclear fuel. Further impregnation experiments using Hf(IV) solution as surrogate of Pu(IV) solution are ongoing to fabricate mixed oxide material. This material will be then analyzed by Energy-dispersive X-ray spectroscopy coupled to transmission electron microscopy to confirm the homogenous distribution of actinides at a nanometric scale.

ACKNOWLEDGMENTS

The authors thank China Scholarship Council (CSC) for the funding of this work. We acknowledge the Laboratoire des Interfaces de Matériaux en Evolution for the use of their facilities.

Author Contributions

Zijie Lu: Investigation, Conceptualization, Methodology, Writing - Original Draft **Thomas Zemb**: Conceptualization, Investigation, Writing, Methodology, Supervision Investigation **Xavier Le Goff**: Investigation **Joseph Lautru**: Investigation **Hassan Khoder**: Investigation **Diane Rébiscoul**: Conceptualization, Investigation, Writing - Original Draft, Methodology, Supervision

REFERENCES

[1] D. Gu, F. Schüth, Synthesis of non-siliceous mesoporous oxides, Chemical Society Reviews 43(1) (2014) 313-344.
[2] D.M. Lyons, L.P. Harman, M.A. Morris, Preparation of a series of mesoporous lanthanide oxides by a neutral supramolecular templating route, Journal of Materials Chemistry 14(13) (2004) 1976-1981.
[3] Y. Castro, B. Julian, C. Boissière, B. Viana, H. Amenitsch, D. Grosso, C. Sanchez, Synthesis, characterization and optical properties of Eu_2O_3 mesoporous thin films, Nanotechnology 18(5) (2007) 055705.
[4] D. Terribile, A. Trovarelli, J. Llorca, C. de Leitenburg, G. Dolcetti, The synthesis and characterization of mesoporous high-surface area ceria prepared using a hybrid organic/inorganic route, Journal of Catalysis 178(1) (1998) 299-308.
[5] C. Reitz, J. Haetge, C. Suchomski, T. Brezesinski, Facile and general synthesis of thermally stable ordered mesoporous rare-earth oxide ceramic thin films with uniform mid-size to large-size pores and strong crystalline texture, Chemistry of Materials 25(22) (2013) 4633-4642.
[6] T. Brezesinski, M. Antonietti, M. Groenewolt, N. Pinna, B. Smarsly, The generation of mesostructured crystalline CeO_2, ZrO_2 and CeO_2–ZrO_2 films using evaporation-induced self-assembly, New Journal of Chemistry 29(1) (2005) 237-242.
[7] R. Zhao, L. Wang, Z.-F. Chai, W.-Q. Shi, Synthesis of ordered mesoporous uranium dioxide by a nanocasting route, Radiochim. Acta 104(8) (2016) 549-553.
[8] G.J.d.A.A. Soler-Illia, C. Sanchez, B. Lebeau, J. Patarin, Chemical strategies to design textured materials: from microporous and mesoporous oxides to nanonetworks and hierarchical structures, Chemical reviews 102(11) (2002) 4093-4138.
[9] G.L. Johnson, L.M. Toth, Plutonium (IV) and thorium (IV) hydrous polymer chemistry, Oak Ridge National Laboratory, Chemistry Division1978.
[10] C. Walther, From hydrolysis to the formation of colloids. Polymerization of tetravalent actinide ions, Forschungszentrum Karlsruhe GmbH Technik und Umwelt (Germany). Inst. fuer …, 2008.
[11] A. Monnier, F. Schüth, Q. Huo, D. Kumar, D. Margolese, R.S. Maxwell, G.D. Stucky, M. Krishnamurty, P. Petroff, A. Firouzi, Cooperative formation of inorganic-organic interfaces in the synthesis of silicate mesostructures, Science 261(5126) (1993) 1299-1303.
[12] Z. Lu, T. Zemb, X. Le Goff, N. Clavier, H. Khoder, J. Lautru, D. Rébiscoul, Facile Preparation of Macro-Microporous Thorium Oxide via a Colloidal Sol–Gel Route toward Safe MOX Fuel Fabrication, ACS Applied Materials & Interfaces (2022).
[13] N. Vlachy, B. Jagoda-Cwiklik, R. Vácha, D. Touraud, P. Jungwirth, W. Kunz, Hofmeister series and specific interactions of charged headgroups with aqueous ions, Advances in colloid and interface science 146(1-2) (2009) 42-47.
[14] H. Meijer, J.K. Smid, Polyether carboxylates, Anionic surfactants: organic chemistry (1996) 314-361.
[15] L. Chiappisi, Polyoxyethylene alkyl ether carboxylic acids: an overview of a neglected class of surfactants with multiresponsive properties, Advances in Colloid and Interface Science 250 (2017) 79-94.
[16] M. Leblanc, J. Causse, Z. Lu, D. Rebiscoul, Stable uranium sols as precursors for the elaboration of nanostructured nc-UO_2 materials, Colloids and Surfaces A: Physicochemical and Engineering Aspects 522 (2017) 18-27.

[17] Z. Lu, J. Lautru, T. Zemb, D. Rébiscoul, Colloidal sol of UO2 nanoparticles supported by multi-lamellar vesicles of carboxylate based surfactant, Colloids and Surfaces A: Physicochemical and Engineering Aspects 603 (2020) 125207.
[18] A. Saravia, Synthesis of carbide fuels from nano-structured precursors: impact on carbo-reduction and physico-chemical properties, Université de Montpellier, 2015.
[19] P. Meakin, Fractal structures, Prog Solid State Ch 20(3) (1990) 135-233.
[20] C.m. Falaise, H.A. Neal, M. Nyman, U(IV) aqueous speciation from the monomer to UO_2 nanoparticles: two levels of control from zwitterionic glycine ligands, Inorganic chemistry 56(11) (2017) 6591-6598.
[21] C.J. Brinker, G.W. Scherer, Sol-gel science: the physics and chemistry of sol-gel processing, Academic press2013.
[22] N. Torapava, I. Persson, L. Eriksson, D. Lundberg, Hydration and Hydrolysis of Thorium(IV) in Aqueous Solution and the Structures of Two Crystalline Thorium(IV) Hydrates, Inorganic Chemistry 48(24) (2009) 11712-11723.
[23] K.E. Knope, R.E. Wilson, M. Vasiliu, D.A. Dixon, L. Soderholm, Thorium (IV) molecular clusters with a hexanuclear Th core, Inorganic chemistry 50(19) (2011) 9696-9704.
[24] K.E. Knope, L. Soderholm, Solution and solid-state structural chemistry of actinide hydrates and their hydrolysis and condensation products, Chemical reviews 113(2) (2013) 944-994.
[25] S. Takao, K. Takao, W. Kraus, F. Emmerling, A.C. Scheinost, G. Bernhard, C. Hennig, First hexanuclear UIV and ThIV formate complexes-Structure and stability range in aqueous solution, European Journal of Inorganic Chemistry 32 (2009) 4771-4775.
[26] Y.J. Hu, K.E. Knope, S. Skanthakumar, L. Soderholm, Understanding the Ligand-Directed Assembly of a Hexanuclear ThIV Molecular Cluster in Aqueous Solution, European Journal of Inorganic Chemistry 2013(24) (2013) 4159-4163.
[27] S. Manet, J. Schmitt, M. Impéror-Clerc, V. Zholobenko, D. Durand, C.L.P. Oliveira, J.S. Pedersen, C. Gervais, N. Baccile, F. Babonneau, Kinetics of the formation of 2D-hexagonal silica nanostructured materials by nonionic block copolymer templating in solution, The journal of physical chemistry B 115(39) (2011) 11330-11344.
[28] Q. Huo, D.I. Margolese, U. Ciesla, D.G. Demuth, P. Feng, T.E. Gier, P. Sieger, A. Firouzi, B.F. Chmelka, Organization of organic molecules with inorganic molecular species into nanocomposite biphase arrays, Chemistry of Materials 6(8) (1994) 1176-1191.
[29] D.L. Parkhurst, C.A.J. Appelo, A computer program for speciation, batch-reaction, one-dimensional transport and inverse geochemical calculations, USGS report (1999).
[30] M. Rand, F.J. Mompean, Chemical thermodynamics, OECD2008.
[31] O. Spalla, S. Lyonnard, F. Testard, Analysis of the small-angle intensity scattered by a porous and granular medium, Journal of applied crystallography 36(2) (2003) 338-347.
[32] E.A. Chavez Panduro, T. Beuvier, M. Fernández Martínez, L. Hassani, B. Calvignac, F. Boury, A. Gibaud, Small-angle X-ray scattering analysis of porous powders of $CaCO_3$, Journal of Applied Crystallography 45(5) (2012) 881-889.
[33] P.D.F. Icdd, International Centre for Diffraction Data, Powder Diffraction File, Newtown Square, Pennsylvania, USA (1997).
[34] D. Grosso, F. Babonneau, C. Sanchez, G.J. de Aa Soler-Illia, E.L. Crepaldi, P.A. Albouy, H. Amenitsch, A.R. Balkenende, A. Brunet-Bruneau, A first insight in the mechanisms involved in the self-assembly of 2D-hexagonal templated SiO_2 and TiO_2 mesostructured films during dip-coating, Journal of sol-gel science and technology 26(1-3) (2003) 561-565.

[35] D. Grosso, G.J. de Aa Soler-Illia, F. Babonneau, C. Sanchez, P.A. Albouy, A. Brunet-Bruneau, A.R. Balkenende, Highly organized mesoporous titania thin films showing mono-oriented 2D hexagonal channels, Advanced Materials 13(14) (2001) 1085-1090.
[36] E.L. Crepaldi, G.J.d.A.A. Soler-Illia, D. Grosso, F. Cagnol, F. Ribot, C. Sanchez, Controlled formation of highly organized mesoporous titania thin films: from mesostructured hybrids to mesoporous nanoanatase TiO_2, Journal of the American Chemical Society 125(32) (2003) 9770-9786.
[37] Y. Wan, D. Zhao, On the controllable soft-templating approach to mesoporous silicates, Chemical reviews 107(7) (2007) 2821-2860.
[38] D. Zhao, Q. Huo, J. Feng, B.F. Chmelka, G.D. Stucky, Nonionic triblock and star diblock copolymer and oligomeric surfactant syntheses of highly ordered, hydrothermally stable, mesoporous silica structures, Journal of the American Chemical Society 120(24) (1998) 6024-6036.
[39] A.R. Massih, Models for MOX fuel behaviour. A selective review, (2006).
[40] K.V.V. Devi, J. Ramkumar, K. Biju, D.B. Sathe, Plutonium heterogeneity in MOX fuel: a quantitative analysis, Journal of Nuclear Materials 518 (2019) 129-139.
[41] T. Yamamoto, Study on double heterogeneity effect of Pu-rich agglomerates in mixed oxide fuel using cross section homogenization method for particle-dispersed media, Annals of Nuclear Energy 37(3) (2010) 398-405.

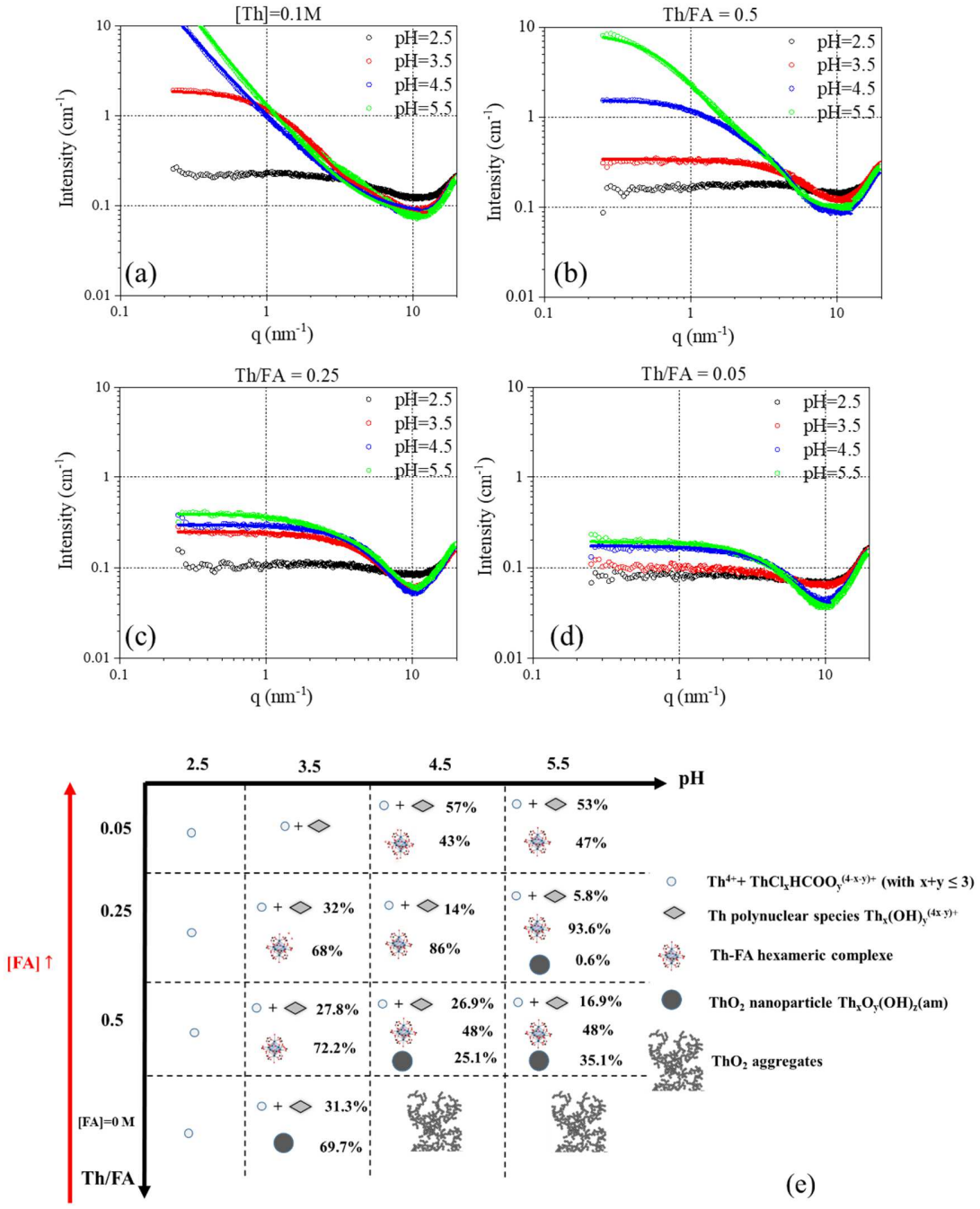

Figure 1. Experimental (dots) and simulated (lines) SAXS patterns at various pH values of (a) the Th solutions at [Th] = 0.1 M, the sols at (b) Th/FA = 0.5, (c) Th/FA = 0.25 and (d) Th/FA = 0.05. (e) Distribution of species in the Th and Th-FA systems as a function of pH and Th/FA molar ratio obtained from the SAXS data simulations.

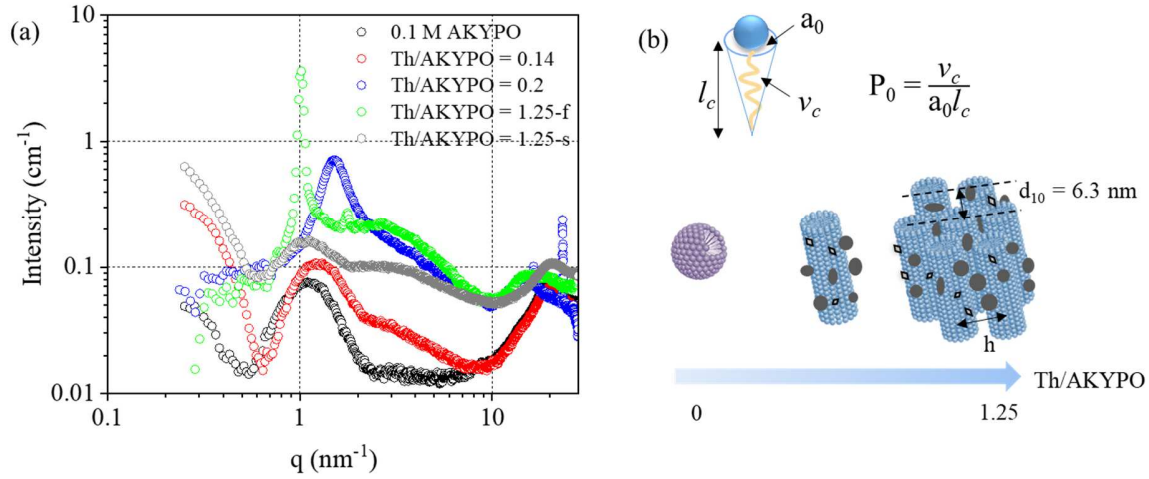

Figure 2. (a) Experimental SAXS patterns of Th-AKYPO sols/floc with various Th/AKYPO ratios. The floc and the supernatant are respectively referred as f and s. (b) Schematic illustration of the phase transition upon the addition of Th solution. d_{10} is the characteristic distance of the first order of scattering and h is the distance between two adjacent cylindrical micelles.

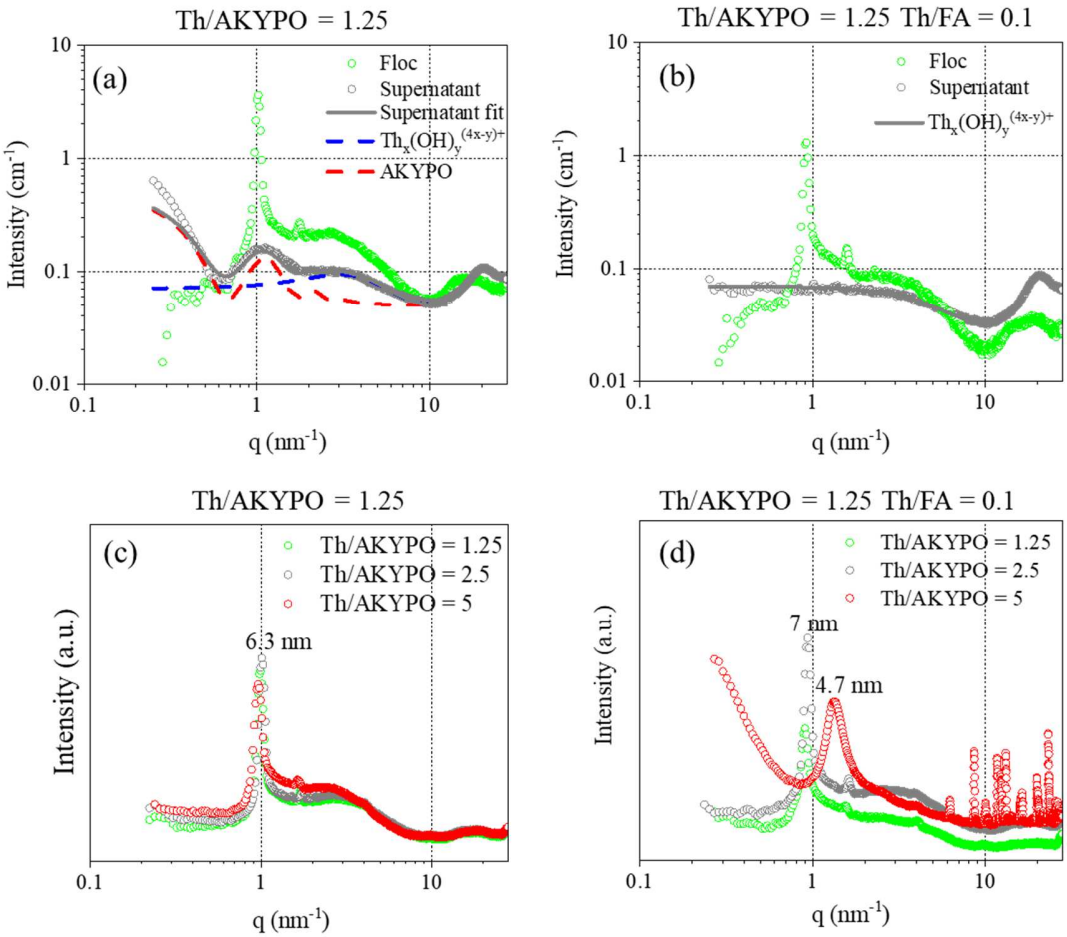

Figure 3. Experimental (dot) and simulated (line) SAXS patterns of the flocs and the supernatants of (a) Th-AKYPO system and (b) Th-FA-AKYPO system with Th/AKYPO = 1.25 and Th/FA = 0.1 for Th-FA-AKYPO. SAXS/WAXS patterns of the flocs with different Th/AKYPO ratios for (c) Th-AKYPO system and (d) Th-FA-AKYPO system (Th/FA = 0.1).

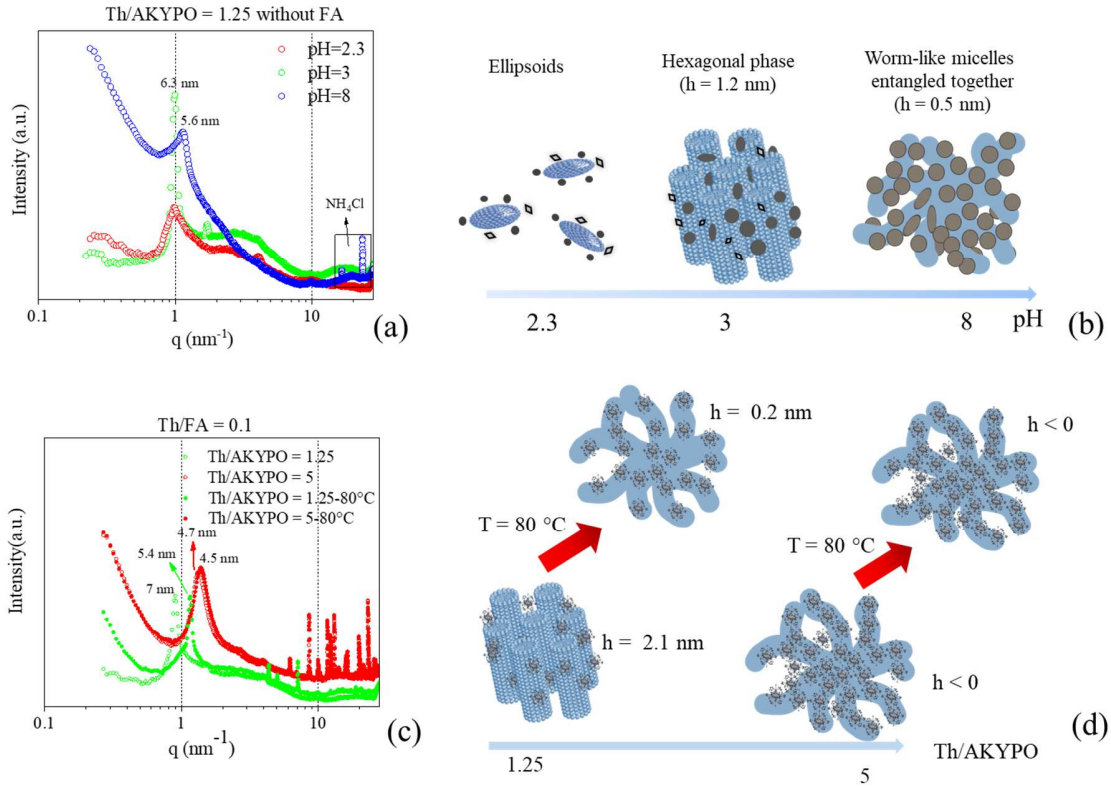

Figure 4. (a) SAXS/WAXS patterns of Th-AKYPO systems at different pH values; (b) schematic illustration of phase transition of Th-AKYPO upon the increase of pH; (c) SAXS/WAXS patterns of Th-FA-AKYPO flocs (Th/FA = 0.1) before and after preheating at 80°C; (d) schematic illustration of the phase transition during the preheating presenting the case of worm-like structure formation (further confirmed by TEM analysis of the final material).

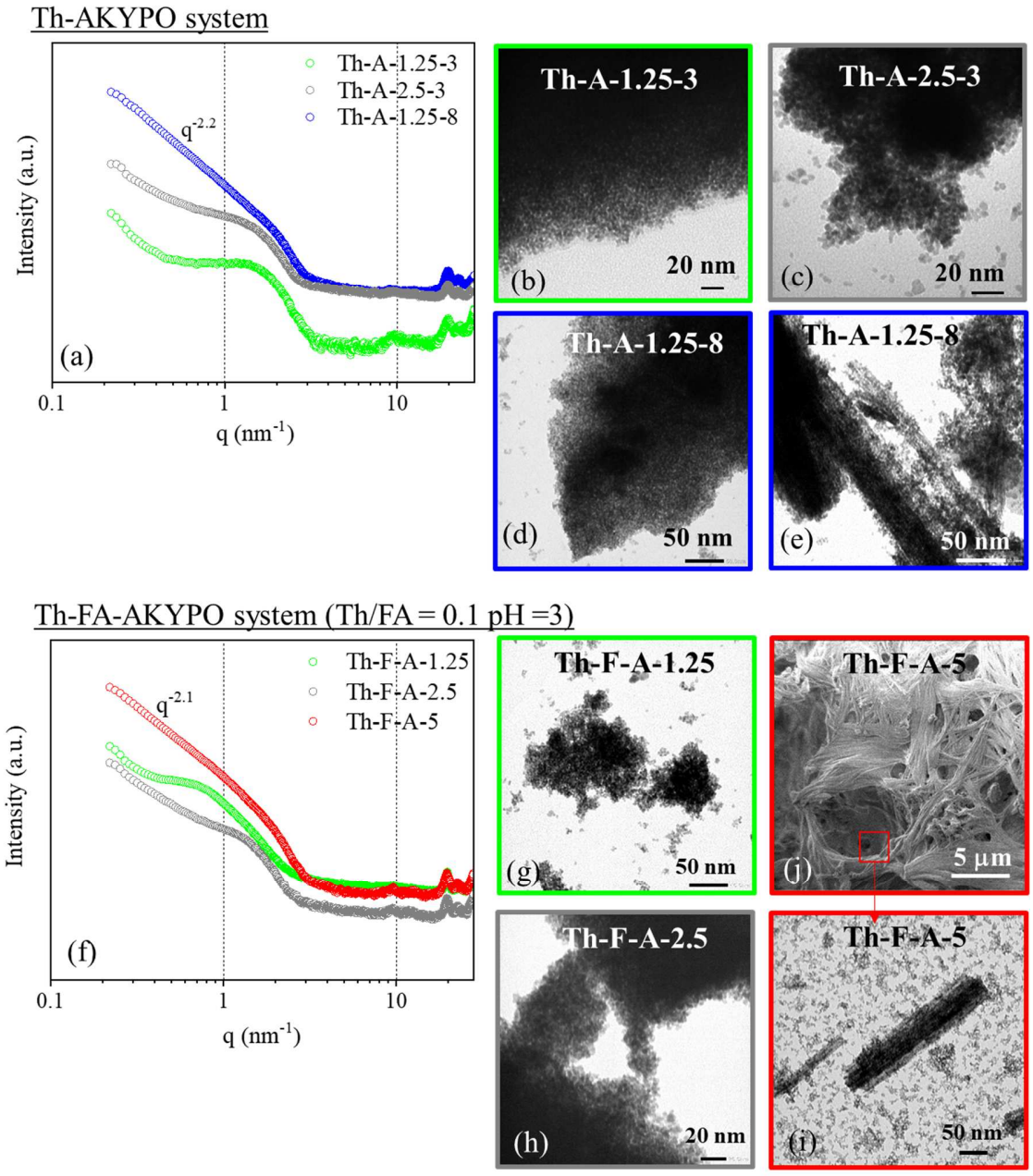

Figure 5. (a) SAXS patterns and TEM images of (b) Th-A-1.25-3, (c) Th-A-2.5-3, (d) and (e) Th-A-1.25-8; (f) SAXS patterns and TEM images of (g) Th-F-A-1.25, (h) Th-F-A-2.5 and (i) Th-F-A-5; (j) SEM image of Th-F-A-5. Th-A-X-Y stands for the final material of Th-AKYPO system prepared with Th/AKYPO = X at pH = Y. Th-F-A-X stands for the final material of Th-FA-AKYPO system prepared with Th/AKYPO = X and Th/FA = 0.1 at pH = 3.

GRAPHICAL ABSTRACT